Parameters Affecting Electron Injection Dynamics from Ruthenium Dyes to Titanium Dioxide Nanocrystalline Thin Film†

John B. Asbury,‡ Neil A. Anderson, Encai Hao,§ Xin Ai, and Tianquan Lian*

Department of Chemistry, Emory University, Atlanta, Georgia 30322

Received: January 19, 2003; In Final Form: April 8, 2003

Electron injection rates from $Ru(dcbpy)_2(X)_2$ [X = 2NCS, 2CN, and dcbpy; dcbpy = 2,2′-bipyridine-4,4′-carboxylate] (called Ru535 or Ru N3, Ru505, and Ru470) to TiO_2 nanocrystalline thin films are examined as a function of adsorbate redox potential, pH of the solution, excitation wavelength, and solvent. For all three dyes, the injection kinetics are biphasic, consisting of a distinct ultrafast component (<100 fs) and slower components. Under different experimental conditions, the partitioning between these two components and the rate of the slow components change, but the rate of the fast component shows no noticeable variations within the ∼200 fs time resolution of the measurement. When Ru535, Ru505, and Ru470 were compared at the same pH, increasing amplitude and decreasing rate of slow component were observed, correlating with less negative excited-state redox potentials in these dyes. An analogous trend was seen for RuN3/TiO_2 by increasing the pH of the solution from pH = 2 to 8 and changing from pH = 2 aqueous solution to a (1:1) ethylene/propylene carbonate mixture. The injection dynamics are also dependent on excitation wavelength. The relative amplitude of the slow component increases when the excitation wavelength is changed from 400 to 630 nm. All data can be described by a two-state injection model, which attributes the fast (<100 fs) component to injection from a nonthermalized excited state and the slow component to injection from the thermalized excited state. The partitioning between these two components and the rate of the slow components depend on the relative energetics between dye excited states and the conduction band edge.

1. Introduction

Because of both applied and fundamental interests, electron-transfer dynamics between molecular adsorbate and semiconductor nanoparticles have been investigated for many years.[1−4] In recent years, ultrafast electron injection from dye sensitizer molecules to nanocrystalline semiconductor thin films has been intensely studied.[5−57] The understanding of these processes is relevant to the design and improvement of Gratzel-type solar cells, for which charge separation and recombination dynamics play a crucial role in determining the overall cell efficiency.[58,59] These systems also provide convenient media for studying ultrafast interfacial electron transfer, a poorly understood fundamental process that is relevant to many semiconductor and metal nanomaterials based devices.

Among many possible combinations of dye and semiconductor materials, solar cells based on $Ru(dcbpy)_2(NCS)_2$ (abbreviated RuN3 or Ru535) sensitized TiO_2 nanocrystalline thin films have produced the highest solar to electric power conversion efficiency.[58,60] For this reason, electron-transfer dynamics in RuN3/TiO_2 system have been studied by many groups.[5−9,19−24,34,36−39,41,42,52,53] There is a general agreement in the literature that photoinduced electron injection from RuN3 to TiO_2 consists of a <100 fs ultrafast component and one or more slower components on the picosecond and longer time scale. However, the magnitude and rate of the slower components vary in results reported by different groups,[5−9,19−22,34,36−39,41,52] and have also been noted to be sensitive to sample conditions.[7] The origin of this discrepancy is so far unclear.

CHART 1: Structure of (a) ReC1 and (b) Ru Dyes

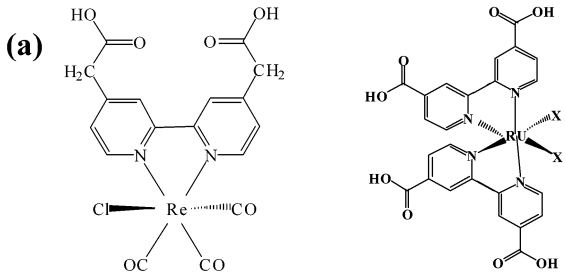

In TiO_2 films sensitized by Ru and Re dyes (see Chart 1), optical excitation with a visible photon at 400−650 nm prepares the molecule to its ^{1}MLCT state, high above the lowest energy ^{3}MLCT state. The excited molecules can undergo electronic relaxation within the excited manifold to the ^{3}MLCT and concurrent intramolecular vibrational energy redistribution and relaxation. For samples in a solvent, solvation relaxation, in which solvent reorganizes to reduce the solvent−solute interaction energy, also occurs.[61−65] The singlet to triplet intersystem crossing time has recently been determined to be ∼75 fs for adsorbed RuN3 on TiO_2 in acetonitrile[36,37] and ∼40 fs[66] and <300 fs[67] for related $Ru(bpy)_3$ in solution. The rate of vibrational relaxation has not been carefully measured, although time constants of a few picoseconds are common for a molecule of this size in solution.[68−70] Our recent study of Re(dcbpy)-$(CO)_3$(Cl) indicates that low-frequency modes that are anhar-

† Part of the special issue "Arnim Henglein Festschrift".

* To whom correspondence should be addressed: e-mail: tlian@emory.edu.

‡ Present address: Department of Chemistry, Stanford University, Stanford, CA.

§ Present address: Department of Chemistry, Northwestern University, Evanston, Illinois 60208.

10.1021/jp034148r CCC: $25.00
Published on Web 05/31/2003

SCHEME 1: Schematic Illustration of Two-State Injection Model[a]

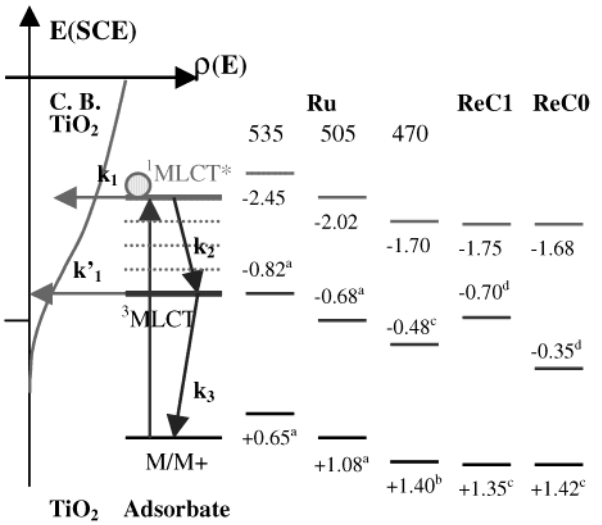

[a] Electron injection (k_1) from nonthermalized excited state competes with intramolecular relaxation (k_2) and the relaxed state injects with a rate constant k_1'. The competition leads to a biphasic injection kinetics (see eq 6 in text). The redox potentials for the ground, excited state (nonrelaxed and relaxed) of dyes are shown to the right. Redox potentials are adopted from (a) ref 52, (b) ref 81, and (d) ref 72 and (c) estimated to be 200 meV less than that of Ru505.[81] Values for the ^{1}MLCT* state are calculated for a 400 nm photon (3.1 eV)

monically coupled to CO stretch modes relax on a few picosecond time scale on ZrO_2 and in solution.[12] A related study of the same dye in alcohol solutions reveals significant solvation dynamics in the excited state on the subpicosecond to a few picoseconds and longer time scale.[71] In light of these excited-state relaxation dynamics of the dye molecule and the <100 fs electron injection component, a significant portion of electron injection must occur from the nonequilibrated excited state. Although this idea has been suggested by many groups,[5−7,9,34,36,37,52] the effects of competition between relaxation and injection pathways on the overall injection kinetics have not been systematically examined.

We previously suggested a two-state injection model to describe the complex injection kinetics caused by the competition between the injection and relaxation pathways.[5,6] In this paper, we expand on this two-state injection model and investigate the parameters that affect the electron injection kinetics in Ru dye-sensitized TiO_2 nanocrystalline thin films. These parameters include the energetics of the dye, pH of solution, solvent, and excitation wavelength.

2. Two-State Electron Injection Model

In Ru and Re dye-sensitized TiO_2 films, optical excitation prepares the molecule to its ^{1}MLCT state, high above the conduction band edge. The molecule undergoes relaxation within the manifold of vibronic excited states in the tens of fs to ps time scale or injects an electron into the semiconductor from any of these unthermalized states. To provide a simple model that captures the main consequence of the two competing pathways, we propose the following two-state injection model.

In this model, we assume that electron injection can occur from an unrelaxed (^{1}MLCT) and relaxed (^{3}MLCT) state as shown in Scheme 1. The unrelaxed state (^{1}MLCT) can inject electrons into semiconductor with a rate constant of k_1 and decay to the relaxed state with a rate constant of k_2. The relaxation rate k_2 incorporates electronic relaxation from singlet to triplet as well as vibrational energy relaxation and solvation stabilization. The relaxed state can inject into the semiconductor with a rate constant of k_1' or decay back to ground state with a rate constant of k_3.

According to this model, the growth of electron population in TiO_2 is given by

$$\frac{d}{dt}N_e(t) = k_1 N^{**}(t) + k_1' N^{*}(t) \tag{1}$$

where $N^{**}(t)$ and $N^{*}(t)$ are the populations of the unrelaxed and relaxed excited states, respectively. These populations change according to the following rate equations:

$$\frac{d}{dt}N^{**}(t) = -(k_1 + k_2)N^{**}(t)$$

$$\frac{d}{dt}N^{*}(t) = -(k_1' + k_3)N^{*}(t) + k_2 N^{**}(t)$$

$$N^{**}(0) = N_0 \qquad N^{*}(0) = 0 \tag{2}$$

where N_0 is the population of the initially excited molecules.

The population of $N^{**}(t)$ and $N^{*}(t)$ can be obtained by solving eq 2:

$$N^{**}(t) = N_0 e^{-(k_1+k_2)t}$$

$$N^{*}(t) = \frac{k_2 N_0}{k_1 + k_2 - k_1' - k_3}[e^{-(k_1'+k_3)t} - e^{-(k_1+k_2)t}] \tag{3}$$

Since the lifetime of the ^{3}MLCT excited state is longer than tens of nanoseconds for these molecules in solution,[60,72] we assume that k_3 is much smaller than k_1, k_1', and k_2. The expression for $N^{*}(t)$ can then be simplified to

$$N^{*}(t) = \frac{k_2 N_0}{k_1 + k_2 - k_1'}[e^{-k_1' t} - e^{-(k_1+k_2)t}] \tag{3a}$$

Substituting the expression for $N^{*}(t)$ and $N^{**}(t)$ into eq 1 and solving for $N_e(t)$, we obtain the kinetics of electron injection:

$$N_e(t) = \frac{k_1 - k_1'}{k_1 + k_2 - k_1'}N_0[1 - e^{-(k_1+k_2)t}] + \frac{k_2}{k_1 + k_2 - k_1'}N_0[1 - e^{-k_1' t}] \tag{4}$$

The expression can be further simplified in the following cases:

Case I. If electron injection from the relaxed state is much slower than that of the unrelaxed state, i.e., $k_1' \ll k_1$ and k_2, then the injection kinetics become

$$N_e(t) = N_0\left\{\frac{k_1}{k_1 + k_2}[1 - e^{-(k_1+k_2)t}] + \frac{k_2}{k_1 + k_2}[1 - e^{-k_1' t}]\right\} \tag{5}$$

This case applies to many of the Ru and Re dye-sensitized TiO_2 systems. Relaxation from the ^{1}MLCT to the ^{3}MLCT state occurs on the <100 fs time scale. The potential for the relaxed ^{3}MLCT state is near the band edge. Because of the rapid decrease in density of conduction band states near the band edge, electron injection from the relaxed state, k_1', is expected to be significantly slower than those from the unthermalized states, k_1.[5,73−75] In the weak coupling limit, the electron injection rate may be expressed as the sum of ET rates to all possible accepting states in the semiconductor. Adopting an approach similar to that of

Marcus and co-workers,[5,74−76] we express the total ET rate from adsorbate to semiconductor:

$$K_{ET} = \frac{2\pi}{h}\int_{-\infty}^{\infty} dE\ \rho(E)|\bar{H}(E)|^2 \frac{1}{\sqrt{4\pi\lambda k_B T}} \exp\left[-\frac{(\lambda + \Delta G_0 - E)^2}{4\lambda k_B T}\right] \quad (6)$$

In eq 3, $\Delta G_0 = E_{CB} - E_{ox}$ is the difference between the potential of conduction band edge and the redox potential of adsorbate excited state; $\rho(E)$ is the density of semiconductor states at energy E from the conduction band edge; $\bar{H}(E)$ is the average electronic coupling between the adsorbate excited state and different k states in the semiconductor at the same energy E; and λ is the total reorganization energy. For simplicity, we assume that in the region of interest, the density of states in semiconductor conduction band is described by a simple band characterized by a nearly-free electron model with effective mass m^* and an exponentially decaying trap state density below the conduction band edge, as illustrated in Scheme 1.

In this case, electron injection kinetics are biphasic, consisting of a fast component with rate constant $k_1 + k_2$ and a slower component with rate constant k_1'. The partitioning between the fast and slow components is determined by ratio of the rate constants k_1/k_2. It is interesting to note that the apparent rise time of the fast component is determined by the fast injection as well as relaxation rate. This has been suggested earlier for Ru dye-sensitized TiO_2 by our group[5,6] and others.[36,37] Furthermore, if k_1' is much slower than 1/(1 ns), then the injection kinetics will appear to consist of only a fast component in our measurement, which extends to about 1 ns. This happens when the relaxed excited state is too far below the conduction band edge, such as the $Re(CO)_3Cl(dcbpy)$ [ReC0]-sensitized TiO_2 system to be discussed later.

Case II. If injection rate constants k_1 and k_1' are much smaller than the relaxation rate within the excited-state levels, i.e., k_1 and $k_1' \ll k_2$, the injection kinetics can be simplified as

$$N_e(t) = N_0(1 - e^{-k_1' t}) \quad (7)$$

In this case, the excited molecules first undergo rapid relaxation within the excited state and electron injection occurs from the relaxed state. The kinetics are no longer distinctly biphasic. This situation can happen when the electronic coupling from the adsorbate to TiO_2 is reduced significantly. $Re(CO)_3Cl(L')$ (L′= 4,4′-diacetate-2,2′-bipyridine) [abbreviated as ReC1] sensitized TiO_2 serves as an example.[13] As will be discussed later, in this system, coupling to TiO_2 was reduced by inserting one CH_2 unit between the anchoring carboxylate group and the bipyridine ligand.

This two-state model is the simplest one that can capture the effect of competition between the injection and relaxation pathways. In reality, electron injection can occur from any states between the initially excited Franck−Condon and fully relaxed ^{3}MLCT state, so a more complete kinetic model should include a continuum of injecting states. However, as long as k_2 is fast, close to the time resolution of the measurement, including more states does not affect qualitatively the injection kinetics. To be more general, the relaxed and unrelaxed state should be interpreted as two regions of states, one near the Franck−Condon state and one near the relaxed state. In this case, k_1 and k_1' are the average injecting rates from the fast and slow injecting regions and k_2 is the rate of relaxation out of the fast injecting regions. Furthermore, a distribution of injection rate k_1', due to an inhomogeneous distribution of dye−semiconductor interaction, should also be considered, which will be discussed later.

3. Experimental Section

Femtosecond Tunable Spectrometer. The tunable femtosecond infrared spectrometer used for our studies was based on a regeneratively amplified femtosecond Ti:sapphire laser system (1 kHz repetition rate at 800 nm, 100 fs, 950 μJ/pulse) and nonlinear frequency mixing techniques. A detailed description of this setup has been presented previously.[12]

The 800 nm output pulse from the regenerative amplifier was split into two parts to generate pump and probe pulses. One part, with 350 μJ/pulse, was used to generate pump pulses at 400 nm by Second Harmonic Generation (SHG) or at 450−650 nm range by a noncollinear optical parametric amplifier (OPA). The 530 and 630 nm pulses had bandwidths of about 30 nm. The remaining 600 μJ of the 800 nm pulse was used to pump an IR optical parametric amplifier to generate two tunable near-IR pulses from 1.1 to 2.5 μm. These signal and idler pulses were combined in an $AgGaS_2$ crystal to generate mid-IR pulses tunable from 3 to 10 μm by difference frequency generation.

After passing through the sample, the mid-infrared probe was spectrally dispersed by an imaging spectrograph and imaged onto a 32 element infrared HgCdTe(MCT) array detector. The amplified outputs of the 32 elements were measured for each pulse. Each element of the array averaged a 2.5 cm^{-1} slice of the infrared spectrum so that the total spectral region covered by the array was ∼80 cm^{-1}. When desired, the spectral resolution could be changed by use of gratings with different dispersion. Transient kinetics at 32 wavelengths were collected simultaneously, from which transient spectra at different delay times were constructed. To minimize low-frequency laser fluctuations, the main noise source, every other pump pulse was blocked with a synchronized chopper (New Focus model 3500) at 500 Hz, and the absorbance change was calculated from two adjacent probe pulses (pump blocked vs unblocked).

The zero delay time and instrument response for a visible pump/mid-IR probe experiment were determined by use of a thin silicon wafer, in which absorption of pump photons leads to the instantaneous generation of charge carriers that absorb strongly in the mid-IR region.[77] The typical instrument response, which was determined in every experiment, could be well represented by a Gaussian function with full width at half-maximum (fwhm) of 200−240 fs.

Materials. High-purity $Ru(dcbpy)_2(X)_2$ (X_2 = 2SCN, 2CN, and dcbpy) [referred to as Ru535 or Ru N3, Ru505, and Ru470, respectively] compounds, shown in Chart 1, were purchased from Solaronix (Lausanne, Switzerland). $Re(CO)_3Cl(dcbpy)$ [ReC0] and $Re(CO)_3Cl(L')$ (L′ = 4,4′-diacetate-2,2′-bipyridine) [ReC1] were prepared in our laboratory.[13] TiO_2 nanocrystalline thin films were prepared by a method similar to that used by Zaban et al.[78] Briefly, TiO_2 nanoparticle colloid was synthesized by controlled hydrolysis of titanium(IV) isopropoxide in a mixture of glacial acetic acid and water at 0 °C. The resulting solution was heated to 80 °C for 8 h and then autoclaved at 230 °C for 12 h. The resulting colloid was concentrated to 150 g/L, spread onto polished sapphire windows, and baked at 400 °C for 36 min. Immersion and storage of the TiO_2 films in a room-temperature ethanol solution containing 200 μM Ru N3 and 20 mM chenodeoxycholic acid resulted in adsorption of the Ru N3 to the porous film surface. The amount of dye coverage on the films was controlled by the time of immersion. The sensitized films were washed with ethanol to remove

unadsorbed dyes. Similar procedures are used for other dyes. These films are either immersed in solvent of interest or exposed to air ("dry film") during the measurements. For pH-dependent study, sensitized films were soaked in a small volume of buffer solution at the desired pH for 24 h prior to study. A small amount of sensitizer can desorb during the soaking process, which was washed away from the films before the experiment. Film samples were moved rapidly during measurement to avoid long-term photoproduct buildup.

4. Results and Discussion

Sensitizer and Semiconductor Energetics. To understand the energy, pH, solvent, and excitation wavelength dependences of the injection dynamics, it is necessary to know the energetics of the sensitizers and semiconductor used in this study. There have been several reports of the ground- and excited-state redox potentials for Ru and Re sensitizers.[42,52,60,72,79−83] A recent comprehensive characterization for Ru and Os polypyridyl complexes was carried out by Sauve et al.[81] The ground-state potentials were measured by cyclic voltammetry. The excited-state potentials were calculated from the ground-state potential and the band origin of ground to ^{3}MLCT transition. The latter was determined by modeling the emission spectrum according to the theoretical model of Meyer and co-workers.[72,84] All values listed in Scheme 1 are for free dyes in solution, which may differ from those of adsorbed dyes.[78,85] Ideally, the latter values should be used, but they are not well determined. Furthermore, these values are also sensitive to solvent and pH because of solvatochromic effect and change of protonation states, respectively.[81] We adopt the latest published values for Ru535, Ru505, and Ru470.[52,81] The value for excited-state redox potential for Ru470 is estimated from that of Ru505 by assuming a 200 meV less negative potential.[81] Despite uncertainty in their absolute values, the relative order of excited-state redox potentials for these dyes, Ru535 < Ru505 < Ru470, is consistent in different reports.[52,60,79−81] We assume similar energetic order for the adsorbed dye. For ReC1 and ReC0, we use the reported values for Re(bpy-CH_3)$(CO)_3$Cl [where bpy-CH_3 = 4,4′-$(CH_3)_2$-2,2′-bipyridine] and Re(bpy-CO_2Et)$(CO)_3$Cl [where bpy-CO_2Et = 4,4′-$(CO_2Et)_2$-2,2′-bipyridine], respectively.[72] The conduction band edge of TiO_2 is −0.52 V at pH = 2 and exhibits a Nernstian shift of −60 meV/increased pH unit.[4,86−89]

IR Absorption Cross-Section Decay for Hot Electrons. One of the predictions of the two-state injection model is that electrons injected from unrelaxed excited state high above conduction band edge have higher kinetic energy than those from the relaxed excited state. Since electron IR absorption is monitored directly in our experiments, the spectral signatures of electrons with different kinetic energies need to be characterized.

The mid-IR absorption of electrons in semiconductor in general contains contributions from free carrier absorption, intraband transitions between different subbands within the conduction or valence bands, and the absorption of trap states.[77] The origin of the mid-IR electron absorption in TiO_2 nanoparticles was investigated in a previous study.[90] It was found that the absorption cross-section increases monotonically with wavelength exhibiting a $\lambda^{1.5}$ dependence in the nanosecond to millisecond time scale. Both free carrier and trap state absorption were possible mechanisms for the observed transition. Free carriers in semiconductor can be excited to a higher energy state by absorbing a photon and simultaneously absorbing or emitting a phonon to conserve momentum.[91] Typically, the free carrier absorption cross-section increases with wavelength, λ^n (n = 2−4), because of the energy dependence of phonon density. The value n depends on the nature of electron−phonon scattering in the materials. On the other hand, the transition cross section from the trap states depends on the overlap of the localized trap state wave function with a delocalized k state in the conduction band. Because of a diminishing contribution of higher k states to the trap state wave function, the transition cross-section also decreases at higher frequency (or momentum).[90,91]

In addition to wavelength dependence, the IR absorption cross-section also depends on the energy of the injected electrons.[91] At the same probe wavelength, the free carrier absorption cross section increases with the temperature or energetics of the electrons due to higher density of states involved in the transitions at higher energy (or k) states. Therefore, if electrons undergo significant energy relaxation, their absorption cross-section is expected to decrease with time.

The measured IR signal depends on the population of the injected electrons, $N_e(t)$, and their average IR absorption cross section, $\sigma(t, \lambda)$:[15,16,18]

$$S_e(t, \lambda) = N_e(t)\sigma(t, \lambda) \tag{8}$$

The population growth reflects the electron injection kinetics, while cross-section change indicates electron relaxation in the semiconductor. To separate population dynamics from absorption cross section, we study adsorbates with strong IR absorption modes, such as ReC0, ReC1, and Fe(II)$(CN)_6^{4-}$, for which population dynamics can be directly measured by monitoring adsorbate vibrational spectral change. Comparing adsorbate signals with electron IR absorption, the electron cross-section decay in TiO_2 can be calculated from eq 8.

Shown in Figure 1a are transient IR spectra of an Fe(II)-$(CN)_6^{4-}$-sensitized TiO_2 thin film in aqueous solution at pH = 2 after 400 nm excitation. Fe(II)$(CN)_6^{4-}$ and TiO_2 form charge-transfer (CT) complexes.[15,16,92,93] Optical excitation of the CT band at 400 nm directly excites an electron from Fe(II)$(CN)_6^{4-}$ to TiO_2, creating a bleach of the ground-state CN stretching mode of Fe(II)$(CN)_6^{4-}$ at 2050 cm^{-1}, and the broad absorption signal of injected electrons in TiO_2. The latter leads to an absorbance increase at all wavelengths in the transient spectrum. A corresponding Fe(III)$(CN)_6^{3-}$ photoproduct absorption band at about 2130 cm^{-1} is also observed but not clearly resolved because of much smaller intensity.[16] The magnitude of the bleach of the CN stretching band reflects the number of injected electrons, since each photoexcited Fe(II)$(CN)_6^{4-}$ generates an injected electron. The magnitude of the IR signal is a product of electron population and average electron absorption cross-section. Shown in Figure 1b is a comparison of these two kinetic traces. The ratio of the electron signal (○) to Fe(II)$(CN)_6^{4+}$ bleach amplitude (− − −) is the relative electron absorption cross section. The calculated normalized cross section is shown in Figure 2. The absorption cross-section decay (●) can be fitted by a double-exponential decay function (—) with time constants and amplitude (in parentheses) of 90 ps (48%) and ≫1 ns (52%).

The redox potential of free Fe(II)$(CN)_6$/Fe(III)$(CN)_6$ couple is at +0.118 V (SCE).[92] However, the value for adsorbed state is not known. The conduction band edge of TiO_2 is −0.52 V (SCE) in aqueous solution of pH = 2.[4] The energy of the injected electron can be estimated from the relationship between optical transition frequency, driving force, and reorganization for a charge-transfer complex.[94] Using a reorganization energy of 1 V for Fe(II)$(CN)_6$,[95], we estimate that the energy of the initially injected electrons created by a 400 nm (3.10 eV) photon is −1.9 V (SCE), significantly above the conduction band edge.

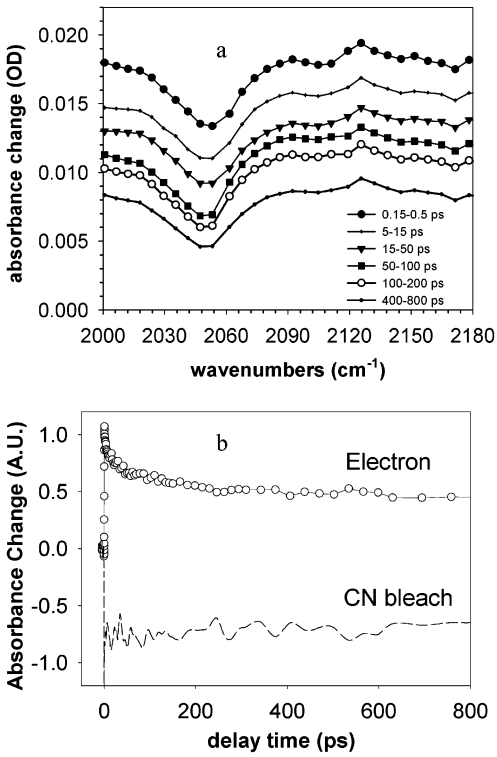

Figure 1. (a) Transient IR difference spectra of $Fe(II)(CN)_6^{4-}$-sensitized TiO_2 film (immersed an aqueous pH = 2 buffer solution) after 400 nm excitation. The spectra are averages of about 10 spectra in the time ranges shown. The broad signal is attributed to injected electrons, and the bleach at 2050 cm^{-1} is assigned to CN stretching mode $Fe(II)(CN)_6^{4-}$. (b) Comparison of the electron signal at 2000 cm^{-1} (○) with CN bleach at 2050 cm^{-1}(− − −).

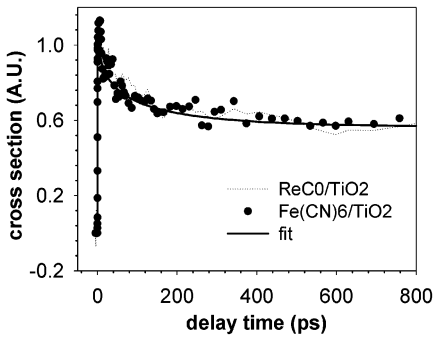

Figure 2. Comparison of electron IR absorption cross section in $Fe(II)(CN)_6^{4-}/TiO_2$ [(●) data; (—) fit] and ReC_0/TiO_2 (•••).

A significant change of density of states is expected as the hot electrons cool to the conduction band edge. We attribute the observed cross section decay to this relaxation process.

In a previous paper we showed that, for ReC0-sensitized TiO_2, the product formation measured by oxidized peak formation does not agree with the electron absorption signal.[13] The oxidized peak showed a <100 fs rise and negligible subsequent change in the <1 ns time scale, indicating <100 fs electron injection and no recombination within 1 ns. However, the electron absorption signal shows a decay characterized by a biexponential function: 90 ps (40%) and ≫1 ns (60%). In this system, 400 nm excitation prepares a Frank−Condon state at ca. −1.68 V (SCE), high above the conduction band edge. The <100 fs injection time and lack of slower injection component suggest that it occurs from the unrelaxed excited state, producing hot electrons. Therefore, the observed decay of the IR signal is attributed to the relaxation of the injected hot electrons. The normalized electron absorption signal, shown by the dotted line in Figure 2, is compared with the hot electron absorption cross section decay measured in $Fe(II)(CN)_6^{4-}/TiO_2$. Within the signal-to-noise of the data, these decay kinetics agree with each other. This observation provides direct evidence for hot electrons injected from the unthermalized excited state, supporting the two-state injection model. The lack of slow injection in ReC0-sensitized TiO_2 is attributed to the low potential of the relaxed excited state, estimated at −0.35V (SCE). This is significantly below the conduction band edge of a dry film, which is not well-known but is expected to be much more negative than −0.74 V, the position at pH = 7, because of its dependence on interfacial proton concentration.[86,88,89,96]

The good agreement between the electron relaxation dynamics in these two systems is somewhat unexpected. The initial kinetic energy of the injected hot electrons in $Fe(II)(CN)_6^{4-}/TiO_2$ is estimated to be around 1.4 V. The value for the $ReC0/TiO_2$ is estimated to be less than 0.94 V, if the conduction edge for a dry film is assumed to be more negative than −0.74 V (SCE). Apparently, within about an 0.5 eV range of kinetic energy difference, hot electron relaxation dynamics are similar within current experimental accuracy. In this paper, we will assume similar hot electron relaxation dynamics for different Ru dyes and different pH. Future experiments that carefully examine how hot electron relaxation dynamics change with excess kinetic energy should be carried out.

For ReC1-sensitized TiO_2, we observed only the slow injection component, characterized by a 20 ps stretched exponential rise.[13] The slower injection rate can be attributed to the reduced electronic coupling introduced by the additional CH_2 group between the bipyridine and the carboxylate anchoring group. In this system, electron injection occurs from its relaxed ^{3}MLCT state at −0.7 V (SCE).[13] Taking into account the reorganization energy involved, the energy of the injected electrons is near or below the conduction band edge. Shown in Figure 3a are transient spectra of $ReC1/TiO_2$ at different delay times after excitation at 400 nm. The spectra are fitted with Gaussian line shapes (solid line) from which the integrated area of the oxidized peak (at 2090 cm^{-1}) is calculated to obtain the population of injected electrons. Shown in Figure 3b is a comparison of the magnitude of the oxidized peak and the IR absorption of electrons. Within the signal-to-noise of the data, these traces agree with each other, suggesting that electrons injected to states near the band edge show no noticeable cross-section decay within 1 ns. Relaxation of electrons to deep trap states either occur on the >1 ns time scale or leads to no noticeable change of IR absorption cross section. A similar measurement for $ReC1/TiO_2$ in aqueous solution of pH = 2 also shows negligible electron cross-section decay. This result will be published elsewhere.

Two-State Electron Injection Model with Electron Cross-Section Decay. For Ru dye-sensitized TiO_2 films to be discussed later, electron IR absorption will be used to follow the injection dynamics, since it is much stronger than those of the adsorbate vibrational modes. The time dependence of the measured electron signal is given by the convolution of population growth and absorption cross-section decay. As discussed in the earlier section, the absorption cross section of slowly injected electrons near the band edge shows no noticeable decays in the <1 ns time scale, while that of electrons injected from unrelaxed state show a 90 ps (48%) decay component. Since this decay of hot electrons is much slower than their <100 fs injection time, the observed electron signal can be simply described by

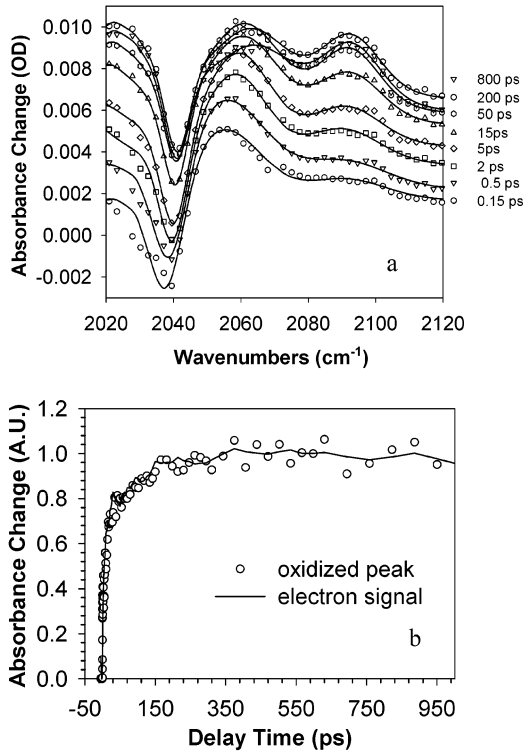

Figure 3. (a) Transient IR absorption spectra of ReC1-sensitized TiO_2 film (exposed to air). (○) Averages of spectra at about 10 delay times around the time indicated; (—) fits of the data to sum of Gaussians. (b) Comparison of normalized oxidized peak area (○) with electron absorption signal (—).

$$S_e(t) = N_0\left\{\frac{k_1}{k_1+k_2}[1-e^{-(k_1+k_2)t}]\sigma_h(t) + \frac{k_2}{k_1+k_2}[1-e^{-k_1't}]\sigma_c\right\} \quad (9)$$

where $\sigma_h(t)$ and σ_c indicate the cross sections for the hot and relaxed electrons.

In the discussion above, we have not taken into account inhomogeneous distribution of adsorbate/nanoparticle interaction. We found in previous studies that when injection was slow enough to be clearly resolved, it was often not single-exponential.[13,14] For this reason, we will fit the slow component using a stretched exponential function. The equation used for fitting the normalized kinetics is then

$$S_e(t) = A(1-e^{-t/\tau_1})c(t) + B(1-e^{-(t/\tau_2)^\alpha}) \quad (10)$$

Comparing with eq 9, we obtain $A/B = (k_1/k_2)[\sigma_h(0)/\sigma_c]$, and $c(t)$ is the normalized cross-section decay function with initial value of 1, given by the fit function in Figure 2. The relative amplitude of the fast and slow components in the observed data depends on the ratios of the fast and slow injection rate constants and the absorption cross sections of these electrons. We further assume that, after the initial relaxation of hot electrons, the absorption cross section at 1 ns is the same as those of slowly injected electrons near the band edge, $\sigma_h(1\text{ ns}) = \sigma_c$. The percentage of injection that occurs from the unrelaxed excited state, $\phi_{inj}^{hot} = k_1/(k_1+k_2)$, can then be calculated from fitting parameters.

Excitation Wavelength Dependence of Electron Injection from Ru N3 to TiO_2. To provide further support for the two-state electron injection model, we studied the pump wavelength dependence of injection dynamics from Ru N3 to TiO_2. If the fast component of electron injection comes from the unrelaxed excited state, by varying the excitation wavelength, we should be able to change the energy of the hot excited state and control the partitioning between the fast and slow injection components.

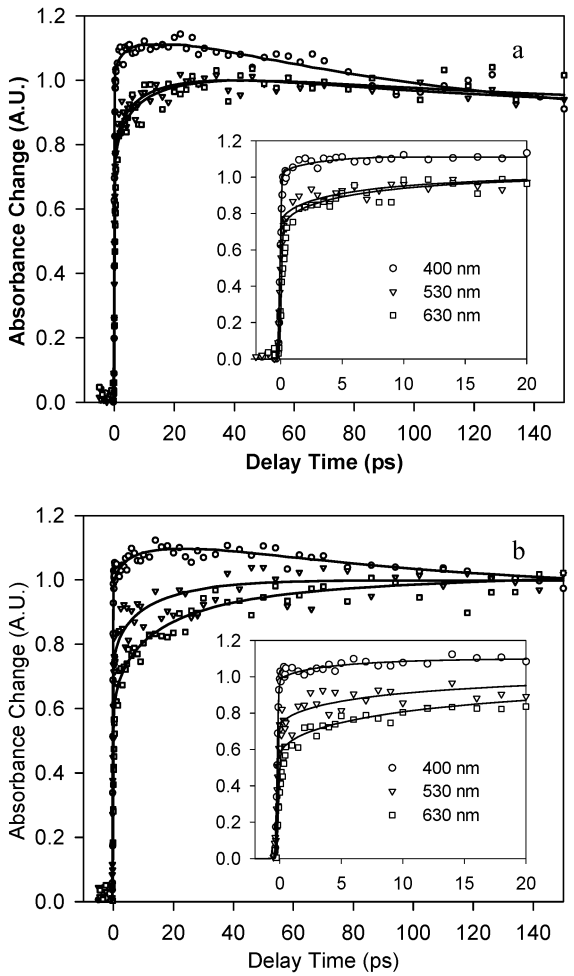

Figure 4. Normalized comparison of electron absorption dynamics of Ru N3- sensitized TiO_2 films after excitation at different pump wavelengths: (a) TiO_2 films at pH = 2; (b) TiO_2 films in ethylene/propylene carbonates (1:1). Insets: The same data plotted on a shorter time scale..

The measured IR absorption kinetics of Ru N3-sensitized TiO_2 films soaked in pH = 2 aqueous buffer solution and an 1:1 ethylene/propylene carbonate mixture (referred to as EC/PC) are shown in Figure 4 panels a and b, respectively. The main panel shows the kinetics traces that correspond to 400 nm (○), 530 nm (▽), and 630 nm (□) pump wavelengths. The kinetics traces have been normalized to have the same signal magnitude at 150 ps. Determination of the absolute magnitude of the signal was hindered by varying beam characteristics at different excitation wavelengths. The insets to the figures show the same data plotted on a shorter time scale. As can be seen for both systems, the percentage of the fast injection component becomes smaller with longer pump wavelengths. This trend is more pronounced in EC/PC than in aqueous solution.

The solid lines are fits to the two-state injection model (eq 10). The fast component is well described by a <100 fs rise and the slow component is fit by a stretched exponential function. The time constant for the slow component changes from 25 ps in pH = 2 water to 50 ps in EC/PC obtained from fitting the kinetics at 400 nm. When comparing different excitation wavelengths within the same solvent, we fixed the time constant and distribution parameter for the slow injection component, since the energy of the relaxed excited state and

TABLE 1: Fitting Parameters of the Electron Injection Dynamics of RuN3-Sensitized TiO_2 at Different Excitation Wavelengths According to Two-State Injection Model[a]

sample	excitation wavelength, nm	fast τ, fs	fast A (%)	slow τ, ps (α)	slow B (%)	ϕ_{inj}^{hot}
TiO_2 at pH = 2	400	<100	75	20 (0.5)	25	0.63
TiO_2 at pH = 2	530	<100	58	20 (0.5)	42	0.44
TiO_2 at pH = 2	630	<100	56	20 (0.5)	44	0.42
TiO_2 in EC/PC	400	<100	66	50 (0.5)	34	0.52
TiO_2 in EC/PC	530	<100	51	50 (0.5)	49	0.37
TiO_2 in EC/PC	630	<100	40	50 (0.5)	60	0.27

[a] The slow components are model by stretched exponential functions with characteristic lifetimes and distribution parameters in parentheses. The fast component is fit by a <100 fs exponential rise. The percentage of injection from unrelaxed state, $\phi_{inj}^{hot} = k_1/(k_1 + k_2)$, is calculated from the ratio A/B after correction for cross section decay.

SCHEME 2: Energetics of Franck−Condon States of Ru535 at Different Excitation Wavelengths and the Conduction Band Edge Positions in Different Solvent

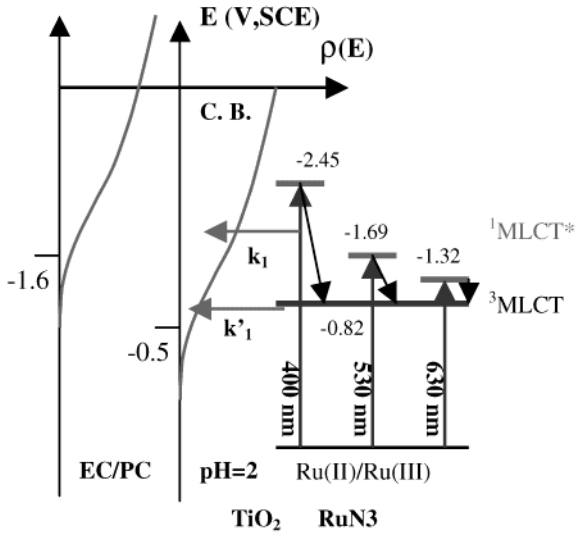

conduction band edge is independent of pump wavelength. The relative amplitudes of fast and slow components are allowed to change. The fitting parameters are summarized in Table 1. The percentage fast injection, ϕ_{inj}^{hot}, is calculated from the amplitudes of the two components used in the fit and the relative cross sections of hot and cooled electrons. As can be seen from Figure 4 and Table 1, with increasing excitation wavelength, the contribution of the fast injection component decreases.

The energetics of relevant states are shown in Scheme 2 for pH = 2 aqueous solution and ethylene/propylene carbonate mixture. By increasing the excitation wavelength, we prepare the unrelaxed state at closer energy to the conduction band edge. As a result, the density of electron-accepting states in TiO_2 decreases, which reduces the electron injection rate from the unthermalized state, k_1. The smaller energy difference between the relaxed and unrelaxed state may also increase the rate of relaxation out of the fast injection region, k_2. Both factors lead to a decrease of the amplitude of the fast injection component. Changing excitation wavelength also results in injection of hot electrons with different kinetic energy, which may lead to different initial absorption cross-section and decay dynamics. This is not accounted for in our current fitting model (eq 10), which assumes the same initial cross section and decay kinetics for hot electrons. This may contribute to some uncertainties in the calculated hot electron injection yield listed in Tables 1 and 2. It should be noted that this is another manifestation of electron injection from the unthermalized excited state. If electrons inject only from the fully thermalized excited state, injection kinetics should be independent of excitation wavelength.

TABLE 2: Fitting Parameters of Electron Injection Dynamics in Sensitized TiO_2 Films[a]

sensitizers	buffer pH	fast component A, %	fast component τ, fs	slow component B, %	slow component τ, ps (α)	k_1/k_2	ϕ_{inj}^{hot}
Ru535	2	73	<100	27	20 (0.5)	1.51	0.60
Ru505	2	55	<100	45	87 (0.5)	0.68	0.41
Ru470	2	~43	<100	~57	~333 (0.5)	~0.42	~0.30
Ru535	2	73	<100	27	20 (0.5)	1.51	0.60
Ru535	4	55	<100	45	60 (0.5)	0.68	0.41
Ru535	6	54	<100	46	100 (0.5)	0.65	0.40
Ru535	8	44	<100	56	130 (0.5)	0.44	0.31

[a] Sensitized by $RuL_2(X)_2$ [2X = 2NCS (Ru535 or Ru N3), 2CN (Ru505), L(Ru470); L = 2,2′-bipyridine-4,4′-bicarboxylate] at pH = 2 and by Ru N3 at different pH values. The slow components are modeled by stretched exponential functions. The fast component is fit by a <100 fs exponential rise. k_1/k_2 is calculated by assuming that $\sigma_c = \sigma_h$ (1 ns). The percentage of injection from unrelaxed state, after correction for cross section decay, is $\phi_{inj}^{hot} = k_1/(k_1 + k_2)$. The data are fit to eq 9.

Excitation wavelength-dependent injection kinetics have also been reported by other groups. Sundstrom and co-workers[36,37] studied Ru N3-sensitized TiO_2 thin films in acetonitrile. With 530 nm excitation, they observed that injection kinetics consists of 60% fast component (~50 fs) and 40% slow components with time constants of ~1, ~10, and ~60 ps. With 455 nm excitation, they observed slightly different injection kinetics, with 70% instantaneous component and 30% slow components. Kuciauskas et al.[52] also observed different injection kinetics at 500 and 560 nm excitation wavelengths. In an earlier study, Durrant et al.[22] showed that injection from Ru N3 to TiO_2 1:1 mixture of ethylene carbonate and propylene carbonate (EC/PC) showed no noticeable difference for excitation wavelengths of 520, 560, and 600 nm. The lack of wavelength dependence in this case may be a result of smaller variation in excitation energy compared to other studies. Change in excitation photon energy is 0.3 eV between 600 and 530 nm and 1.1 eV between 400 and 630 nm. Our data also showed that injection kinetics differences between 530 and 630 nm excitation are small in PC/EC solution and not even noticeable in aqueous pH = 2 solution.

Observation of different electron cross-section decay for fast (ReC0) and slow (ReC1) injection components as well as excitation wavelength-dependent injection dynamics support the two-state injection model. It will be used to describe the dependence of injection kinetics on adsorbate redox potential, pH, and solvent.

Comparison of Injection Dynamics in Different Ru Dyes at pH = 2. Shown in Figure 5 is a comparison of electron injection kinetics of different Ru dye-sensitized TiO_2 films submerged in aqueous buffer solution of pH = 2. The signal sizes have been normalized at 150 ps. The inset shows the same data on a shorter time scale and with the fast component cropped to highlight the difference of the slow components. On going from Ru535 to Ru505 to Ru470, the relative amplitude of the fast component decreases, and the slow component becomes slower. The solid lines are fits to the two-state injection model described earlier (eq 10), consisting of a fast (<100 fs) exponential, convoluted with cross-section decay, and a slow stretched exponential rise. To facilitate comparison of time scales, the same stretched exponential distribution factor α of

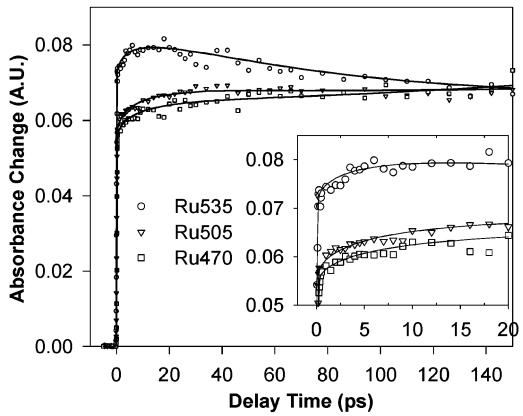

Figure 5. Normalized comparison of electron injection dynamics of Ru535-, Ru505-, and Ru470-sensitized TiO_2 films at pH = 2. Solid lines are fits according to eq 10, consisting of a fast (<100 fs) exponent rise with cross section decay and a slower stretched exponential rise component (see Table 2 for fit parameters). The inset shows the same data in a shorter time scale.

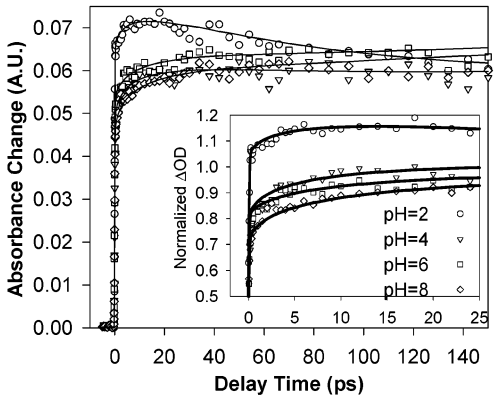

Figure 6. Comparison of electron absorption dynamics of Ru N3-sensitized TiO_2 films at different pH values. Symbols indicate data; solid lines are fits according to eq 10. Inset: comparison of the same data normalized to 1 at 150 ps. The fast injection component has been cropped out of the figure and a shorter time scale is shown to highlight the difference.

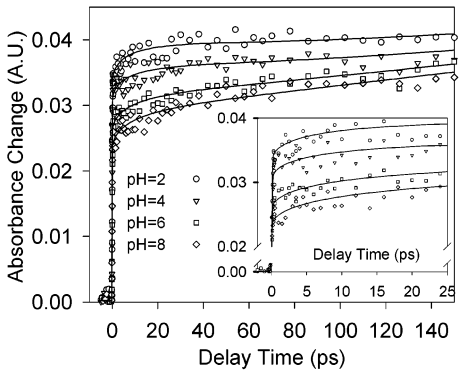

Figure 7. Comparison of electron absorption dynamics of Ru470-sensitized TiO_2 films at different pH values. Symbols indicate data; solid lines are fits according to eq 10. Inset: the same data plotted on a shorter time scale.

0.5 was used for all data. The parameters used for the fit are shown in Table 2. It should be noted here that the time constant of the slow component is not very accurately determined for Ru470 because of the signal is still increasing at 150 ps, the longest delay time measured.

All these dyes are attached to TiO_2 through the dcbpy ligand. They differ in the third coordination ligand, which leads to significant changes in their ground and excited-state redox potential, as shown in Scheme 1. From Ru535 and Ru505 to Ru470, the excited-state redox potential become less negative. We suggest that as the unrelaxed state becomes closer to the band edge, injection rate k_1 may decrease due to reduced density of accepting states in TiO_2, and the rate of relaxation out of the fast injection region, k_2, may increase. Both factors lead to a reduced fast injection component according to the two-state injection model (eqs 9 and 10). The rate of the fast component, $k_1 + k_2$, may also change, but because it is faster than our time resolution, any small difference may not be resolved in the current experiment. The trend was more clearly demonstrated in our previous comparison of the same series of Ru dyes on dry TiO_2 films, in which systematic decrease of fast component amplitude was also observed.[5,6]

The trend in the rate of slow injection component is also consistent with this model. In going from Ru535 to Ru470, the relaxed states are at increasingly less negative potential and their corresponding density of electron-accepting states in TiO_2 decreases, leading to increasingly slower electron injection. In comparing the trend of injection kinetics observed in different Ru dyes, we have assumed that the main difference in these dyes is caused by their energetics. It is unclear how much electronic coupling between the dcbpy π^* orbital and TiO_2 changes in these dyes. To further test the energy dependence of the injection kinetics, we studied the pH dependence of the electron injection process from Ru535 and Ru470 to TiO_2.

pH Dependence of Electron Injection. The electron injection dynamics of Ru N3-sensitized TiO_2 films soaked in aqueous buffer solutions of different pH are compared in Figure 6. Signal magnitudes at each pH have been scaled to correct for small optical density differences in the films at 400 nm. The corrected signal sizes of $RuL_2(NCS)_2$ at different pH values are approximately the same, indicating similar electron injection efficiency. The inset shows a comparison of the data that have been normalized at 150 ps. These are displayed on a shorter time scale to highlight the difference in the slow components. The amplitude of the fast component decreases and that of the slow component increases at higher pH.

The solid lines through the data are fits to eq 10, and the fitting parameters are listed in Table 2. The fast components are well described by <100 fs exponential rise function at all pH values. The slow components varied in time scale from 20 ps at pH = 2 to 130 ps at pH = 8, a factor of 6 difference between the two extremes. The percentage of fast injection (after correction of cross-section decay) is calculated from the fitting parameters and compared in Table 2.

The electron injection dynamics of Ru470-sensitized TiO_2 films soaked in aqueous buffer solutions of different pH are compared in Figure 7. The data are measured and analyzed in the same way as that of Ru N3 shown in Figure 6. The fast components are well described by <100 fs exponential rise function. The slow components become slower with increasing pH, although they are much too slow to be accurately determined within the limited delay times of the measurement. The amplitude of the fast component decreases at higher pH. The total signal size at 150 ps becomes smaller at higher pH. Since the slow component appears to be not completed at 150 ps at higher pH, and if we assume the same injection yield is reached at longer delay time, the results suggest that relative amplitude of the slow component becomes larger at higher pH.

It has been well established that in aqueous solution the TiO_2 conduction band edge moves to more negative potentials by 60 meV/increased pH unit.[86,88,89,96] However, it is less clear how

the redox potential of the adsorbed dye changes with pH. It may be affected by changes in the protonation state of the dcbpy ligand[97] as well as potential drop at the interface.[78,85] The latter effect was recently shown to depend on the size of the adsorbate and cation at the interface.[78,85] pK_a values for the first and second protonation steps are 3 and 1.5, respectively. Furthermore, the interaction of the carboxylate group with TiO_2 may also change at different pH.[40] We have recently studied the pH dependence of ReC1 on TiO_2. In this system, the injection rate changes from about 20 ps in pH = 2 to a few hundred picoseconds at pH = 8 (result to be published elsewhere). It appears that in this system the decrease of injection rate at higher pH can be accounted for by the reduction of the density of electron-accepting states in TiO_2 caused by the shifting the conduction band edge to more negative potentials.

To understand the pH dependence of injection dynamics in Ru N3-sensitized TiO_2, we assume that the dominating effect of increasing pH is also changing the conduction band edge to more negative values. At higher pH, the conduction band edge moves closer to the unrelaxed state, slowing down k_1 and thus reducing the amplitude of the fast component. For the same reason, the injection rate from the relaxed state also slows down, consistent with the experimental observation. It is unclear how much dye energetics or coupling change over this pH range. In future experiments, we would like to study the dependence over a wider pH value.[98]

More pronounced pH dependence of injection kinetics is observed in Ru470-sensitized TiO_2. In addition, the rate of the slow injection component is slower than those in Ru535/TiO_2. Compared to Ru535, the excited-state energetics of Ru470 is closer to the band edge. The relaxed state, estimated at −0.5 V (SCE),[52,81] is slightly below the band edge at pH = 2. Taking into account reorganization energy, the accepting states in TiO_2 are most likely trap states below the band edge, which leads to a much slower injection rate compared to Ru535, as shown in Figure 5. Another consequence is that the slow components are much more sensitive to pH because of the exponentially decaying density of states in this region.

The dependence of injection dynamics on pH and cation concentration in solution has been examined in previous studies.[19,40,41] Durrant and co-workers[19] found that that injection rate of Ru535/TiO_2 in CH_3CN depended on the concentration of Li^+ cation. Under −0.2 V external bias, the injection rate in pure CH_3CN is significantly slower than that in the presence of 0.1 M $LiClO_4$, although the total yield is similar. Meyer and co-workers[40,41] examined the dependence of luminescence quantum yield on cation concentration and pH in Ru dye-sensitized TiO_2 film. At higher cation or proton concentration, they observed decreased sensitizer luminescence quantum yield, which suggests faster electron-transfer rates. These dependences were attributed to the shifting of empty electron-accepting states in semiconductor as a function of proton or cation concentration, consistent with our observation.

It appears that the same trend of change in injection dynamics is observed either by lowering the dye excited-state redox potential down toward the conduction band edge (comparing different dyes at the same pH) or by raising the conduction band (comparing the same dye at different pH). This suggests that the most important factor for injection dynamics in these Ru dye-sensitized TiO_2 is the relative energetics between the dye and semiconductor.

Solvent Dependence. As shown in Figure 4 and Table 1, the injection dynamics in EC/PC are different from those in pH = 2 aqueous solution for the same excitation wavelength. The amplitude of fast component is smaller and the rate of the slow component is reduced. Changing the solvent has two effects on the electron-transfer rate. First, solvent reorganization energy varies in solvents of different dielectric constant. Formally, within the dielectric continuum model, solvent reorganization energy can be calculated from the dielectric constant of the solvent at the interface.[99−101] The static and optical dielectric constants are 114 and 6.3 for TiO_2, 78 and 1.78 for water, and 65 and 2.2 for propylene carbonate. We assume a spherical cavity of r = 6.8 Å for Ru N3 similar to that of $Ru(bpy)_3^{2+}$[102] and the distance to the surface $d = r$. Using the formula by Marcus,[99] we estimate that solvent reorganization energy changes from 0.42 eV in water to 0.38 eV in propylene carbonate.

Change of solvent can also affect the energetics of the adsorbate and the semiconductor. The flat band potential of nanocrystalline TiO_2 films soaked in ethylene carbonate has been measured to be about −1.6 V (vs SCE),[89] about 1.1 V higher in energy than the potential of the same film in pH = 2 water.[87,89] However, band edge position in nonaqueous solution was found to be very sensitive to water content because of preferential adsorption of water at the TiO_2 surface.[89] We suspect that the band edge position of our sample in EC/PC may be less negative than −1.6 V (but more negative than −0.5 V) because some amount of water may exist. As illustrated in Scheme 2, in EC/PC, the densities of electron-accepting states for injection from both the unrelaxed and relaxed states are smaller because of the more negative conduction band edge position. As a result, both k_1 and k_{-1} decrease, reducing the amplitude of the fast injection component and the rate of slow component.

The observed trend in these two solvents (see Table 2) is consistent with the effect of changing relative energetics of the adsorbate and conduction band edge. However, it is difficult to quantify the relative contributions of change in reorganization energy vs energetics from the current set of measurements. These questions will be investigated in future solvent dependence studies.

Solvent dependence of electron injection dynamics from Ru N3 to TiO_2 films has been studied.[22] Indistinguishable nonexponential injection dynamics in films soaked in a mixture of ethylene and propylene carbonates, in acetonitrile, or in ethanol and dried in air were observed. Solvents investigated in our study span a larger range of proton concentration and effect a bigger change in conduction band edge position, which may lead to a more noticeable difference in injection kinetics.

Summary

We have examined parameters that affect electron injection rate from Ru N3 and related dyes to TiO_2 nanocrystalline thin film. These parameters include excitation wavelength, dye energetics, pH of the solution, and the solvent. For Ru535, Ru505, and Ru470 on TiO_2 under varying pH, excitation wavelength, and solvent, the injection kinetics are biphasic, consisting of a distinct ultrafast component (<100 fs) and slower components. Under different experimental conditions, the relative amplitude and rate of slow components changes but the rate of the fast component shows no noticeable variations, probably due to limited time resolution of the measurement. All data can be accounted for by a two-state injection model in which the fast (<100 fs) component arises from injection from the nonthermalized excited state and the slow component corresponds to injection from the relaxed excited state. According to this model, the rate of the fast component is determined

by the sum of the rate constants of injection from the nonthermalized state, k_1, and relaxation to the thermalized excited state, k_2. Both of these processes are faster than $(100\ fs)^{-1}$ for Ru dyes/TiO_2 and the resulting rate of fast component is $>(100\ fs)^{-1}$ in all cases, which cannot be differentiated within our time resolution. The relative magnitude of the fast and slow injection components increases with the ratio of the rate constants (k_1/k_2) for these processes. The rate of the slow injection component depends on the relative energetics of the adsorbate vs conduction band edge following the change of density of accepting states in the semiconductor.

Injection of hot electrons from the unthermalized excited state is directly observed experimentally by monitoring the electron IR absorption cross-section decay. Excitation wavelength-dependent injection dynamics were observed, lending further support to the two-state injection model. The observed dependence on energetics, pH, excitation wavelength, and solvent is consistent with the two-state injection model. On changing the excitation wavelength from 400 to 630 nm, we observed a reduction of the relative amplitude of the fast component. With increasing excitation wavelengths, the unrelaxed excited states are at less negative potential, closer to the conduction band edge. This leads to a decrease of the amplitude of the fast component. On going from Ru535 and Ru505 to Ru470, we observed that the amplitude of fast component decreased and the rate constant for the slow component slowed. This is attributed to the change of energetics of the adsorbate. When these three dyes are compared, both the unrelaxed and relaxed excited states become less negative (closer to band edge) from Ru 535 to Ru470. According to the two-state injection model, this leads to the reduction of k_1/k_2 and decrease of the rate constant for the slow injection component. On increasing pH, we observed that the amount of fast component decreased and the rate of slow component decreased for both Ru535 and Ru470. This is attributed to the shifting of conduction band edge to more negative potentials at higher pH. This effect leads to a similar change of relative energetics of adsorbate and semiconductor compared to the three Ru dyes at the same pH. Therefore, the same trend of change in the injection dynamics was observed. In comparing the injection dynamics of pH = 2 aqueous solution and EC/PC mixture, we found that at the same excitation wavelength the injection dynamics in the latter solvent has a smaller amplitude for the fast component and a slower rate for the slow component. This is consistent with the more negative conduction band edge expected in the EC/PC mixture.

Electron injection dynamics from Ru N3 to TiO_2 have been examined by different groups.[5−9,19−22,34,36−39,41,52] We showed here that excitation wavelength has a noticeable effect on the relative amplitude of fast and slow component and the solvent environment affects both the relative amount and rate constant of the slow components because of the change of relative energetics between dye excited state and conduction band edge. We suggest that the small difference of the reported injection kinetics by different groups may be in part due to the variance in experimental conditions, namely, the excitation wavelength and the solvent environment.

Acknowledgment. We thank the Division of Chemical Sciences, Office of Basic Energy Research, U.S. Department of Energy, for financial support. This work is also supported in part by the donors of the Petroleum Research Fund and Emory University Research Committee. We thank Drs. Yongqiang Wang (Figure 3) and Hiren N. Ghosh (Figure 1) for their contribution in the early stage of this work. T.L. is an Alfred P. Sloan fellow.

References and Notes

(1) Miller, R. J. D.; McLendon, G. L.; Nozik, A. J.; Schmickler, W.; Willig, F. *Surface electron-transfer processes*; VCH Publishers, Inc.: New York, 1995.
(2) Kamat, P. V. *Prog. Reaction Kinet.* **1994**, *19*, 277.
(3) Kamat, P. V. *Chem. Rev.* **1993**, *93*, 267.
(4) Hagfeldt, A.; Gratzel, M. *Chem. Rev.* **1995**, *95*, 49.
(5) Asbury, J. B.; Hao, E.; Wang, Y.; Ghosh, H. N.; Lian, T. *J. Phys. Chem. B* **2001**, *105*, 4545.
(6) Asbury, J. B.; Wang, Y. Q.; Hao, E. C.; Ghosh, H. N.; Lian, T. *Res. Chem. Intermed.* **2001**, *27*, 315.
(7) Asbury, J. B.; Ellingson, R. J.; Ghosh, H. N.; Ferrere, S.; Nozik, A. J.; Lian, T. *J. Phys. Chem. B* **1999**, *103*, 3110.
(8) Ellingson, R. J.; Asbury, J. B.; Ferrere, S.; Ghosh, H. N.; Sprague, J. R.; Lian, T.; Nozik, A. J. *Z. Phys. Chem. (Muenchen)* **1999**, *212*, 77.
(9) Ellingson, R. J.; Asbury, J. B.; Ferrere, S.; Ghosh, H. N.; Sprague, J. R.; Lian, T.; Nozik, A. J. *J. Phys. Chem. B* **1998**, *102*, 6455.
(10) Ghosh, H. N.; Asbury, J. B.; Lian, T. *PINSA-A: Proc. Indian Natl. Sci. Acad., Part A* **2000**, *66*, 177.
(11) Anderson, N. A.; Hao, E.; Ai, X.; Hastings, G.; Lian, T. *Chem. Phys. Lett.* **2001**, *347*, 304.
(12) Wang, Y.; Asbury, J. B.; Lian, T. *J. Phys. Chem. A* **2000**, *104*, 4291.
(13) Asbury, J. B.; Hao, E.; Wang, Y.; Lian, T. *J. Phys. Chem. B* **2000**, *104*, 11957.
(14) Asbury, J. B.; Wang, Y.; Lian, T. *J. Phys. Chem. B* **1999**, *103*, 6643.
(15) Weng, Y.-X.; Wang, Y.-Q.; Asbury, J. B.; Ghosh, H. N.; Lian, T. *J. Phys. Chem. B* **2000**, *104*, 93.
(16) Ghosh, H. N.; Asbury, J. B.; Weng, Y.; Lian, T. *J. Phys. Chem. B* **1998**, *102*, 10208.
(17) Ghosh, H. N.; Asbury, J. B.; Lian, T. *J. Phys. Chem. B* **1998**, *102*, 6482.
(18) Hao, E.; Anderson, N. A.; Asbury, J. B.; Lian, T. *J. Phys. Chem. B* **2002**, *106*, 10191.
(19) Tachibana, Y.; Haque, S. A.; Mercer, I. P.; Moser, J. E.; Klug, D. R.; Durrant, J. R. *J. Phys. Chem. B* **2001**, *105*, 7424.
(20) Tachibana, Y.; Haque, S. A.; Mercer, I. P.; Durrant, J. R.; Klug, D. R. *J. Phys. Chem. B* **2000**, *104*, 1198.
(21) Tachibana, Y.; Moser, J. E.; Graetzel, M.; Klug, D. R.; Durrant, J. R. *J. Phys. Chem.* **1996**, *100*, 20056.
(22) Durrant, J. R.; Tachibana, Y.; Mercer, I.; Moser, J. E.; Gratzel, M.; Klug, D. R. *Z. Phys. Chem.* **1999**, *212*, 93.
(23) Haque, S. A.; Tachibana, Y.; Willis, R. L.; Moser, J. E.; Graetzel, M.; Klug, D. R.; Durrant, J. R. *J. Phys. Chem. B* **2000**, *104*, 538.
(24) Haque, S. A.; Tachibana, Y.; Klug, D. R.; Durrant, J. R. *J. Phys. Chem. B* **1998**, *102*, 1745.
(25) Bach, U.; Tachibana, Y.; Moser, J.-E.; Haque, S. A.; Durrant, J. R.; Graetzel, M.; Klug, D. R. *J. Am. Chem. Soc.* **1999**, *121*, 7445.
(26) Nogueira, A. F.; De Paoli, M.-A.; Montanari, I.; Monkhouse, R.; Nelson, J.; Durrant, J. R. *J. Phys. Chem. B* **2001**, *105*, 7517.
(27) Ramakrishna, S.; Willig, F.; May, V. *Chem. Phys. Lett.* **2002**, *351*, 242.
(28) Zimmermann, C.; Willig, F.; Ramakrishna, S.; Burfeindt, B.; Pettinger, B.; Eichberger, R.; Storck, W. *J. Phys. Chem. B* **2001**, *105*, 9245.
(29) Ramakrishna, S.; Willig, F.; May, V. *J. Chem. Phys.* **2001**, *115*, 2743.
(30) Ramakrishna, S.; Willig, F. *J. Phys. Chem. B* **2000**, *104*, 68.
(31) Ramakrishna, S.; Willig, F.; May, V. *Phys. Rev. B: Condens. Matter Mater. Phys.* **2000**, *62*, R16330.
(32) Burfeindt, B.; Zimmermann, C.; Ramakrishna, S.; Hannappel, T.; Meissner, B.; Storck, W.; Willig, F. *Z. Phys. Chem. (Muenchen)* **1999**, *212*, 67.
(33) Burfeindt, B.; Hannapel, T.; Storck, W.; Willig, F. *J. Phys. Chem.* **1996**, *100*, 16463.
(34) Hannappel, T.; Burfeindt, B.; Storck, W.; Willig, F. *J. Phys. Chem. B* **1997**, *101*, 6799.
(35) Hilgendorff, M.; Sundstrom, V. *Chem. Phys. Lett.* **1998**, *287*, 709.
(36) Banko, G.; Kalloinen, J.; Korppi-Tommola, J. E. I.; Yartsev, A. P.; Sundstrom, V. *J. Am. Chem. Soc.* **2002**, *124*, 489.
(37) Kalloinen, J.; Banko, G.; Sundstrom, V.; Korppi-Tommola, J. E. I.; Yartsev, A. P. *J. Phys. Chem. B* **2002**, *106*, 4396.
(38) Heimer, T. A.; Heilweil, E. J.; Bignozzi, C. A.; Meyer, G. J. *J. Phys. Chem. A* **2000**, *104*, 4256.
(39) Heimer, T.; Heilweil, E. J. *J. Phys. Chem. B* **1997**, *101*, 10990.
(40) Qu, P.; Meyer, G. J. *Langmuir* **2001**, *17*, 6720.
(41) Kelley, C. A.; Farzad, F.; Thompson, D. W.; Stipkala, J. M.; Meyer, G. J. *Langmuir* **1999**, *15*, 7047.

(42) Hasselmann, G. M.; Meyer, G. J. *J. Phys. Chem. B* **1999**, *103*, 7671.
(43) Hasselmann, G. M.; Meyer, G. J. *Z. Phys. Chem. (Muenchen)* **1999**, *212*, 39.
(44) Farzad, F.; Thompson, D. W.; Kelly, C. A.; Meyer, G. J. *J. Am. Chem. Soc.* **1999**, *121*, 5577.
(45) Butoi, C. I.; Langdon, B. T.; Kelley, D. F. *J. Phys. Chem. B* **1998**, *102*, 9635.
(46) Langdon, B. T.; MacKenzie, V. J.; Asunskis, D. J.; Kelley, D. F. *J. Phys. Chem. B* **1999**, *103*, 11176.
(47) Chikan, V.; Waterland, M. R.; Huang, J. M.; Kelley, D. F. *J. Chem. Phys.* **2000**, *113*, 5448.
(48) Martini, I.; Hodak, J. H.; Hartland, G. V. *J. Phys. Chem. B* **1998**, *102*, 607.
(49) Martini, I.; Hodak, J. H.; Hartland, G. V. *J. Phys. Chem. B* **1998**, *102*, 9508.
(50) Martini, I.; Hodak, J.; Hartland, G. V.; Kamat, P. V. *J. Chem. Phys.* **1997**, *107*, 8064.
(51) Cherepy, N. J.; Smestad, G. P.; Gratzel, M.; Zhang, J. Z. *J. Phys. Chem.* **1997**, *101*, 9342.
(52) Kuciauskas, D.; Monat, J. E.; Villahermosa, R.; Gray, H. B.; Lewis, N. S.; McCusker, J. K. *J. Phys. Chem. B* **2002**, *106*, 9347.
(53) Kuciauskas, D.; Freund, M. S.; Gray, H. B.; Winkler, J. R.; Lewis, N. S. *J. Phys. Chem. B* **2001**, *105*, 392.
(54) Lanzafame, J. M.; Palese, S.; Wang, D.; Miller, R. J. D.; Muenter, A. A. *J. Phys. Chem.* **1994**, *98*, 11020.
(55) Lanzafame, J. M.; Miller, R. J. D.; Muenter, A.; Parkinson, B. *J. Phys. Chem.* **1992**, *96*, 2820.
(56) Rehm, J. M.; McLendon, G. L.; Nagasawa, Y.; Yoshihara, K.; Moser, J.; Gratzel, M. *J. Phys. Chem.* **1996**, *100*, 9577.
(57) Stier, W.; Prezhdo, O. V. *J. Phys. Chem. B* **2002**, *106*, 8047.
(58) O'Regan, B.; Gratzel, M. *Nature* **1991**, *353*, 737.
(59) Bach, U.; Lupo, D.; Comte, P.; Moser, J. E.; Weissortel, F.; Salbeck, J.; Spreitzer, H.; Gratzel, M. *Nature* **1998**, *395*, 583.
(60) Nazeeruddin, M. K.; Kay, A.; Rodicio, I.; Humphrybaker, R.; Muller, E.; Liska, P.; Vlachopoulos, N.; Gratzel, M. *J. Am. Chem. Soc.* **1993**, *115*, 6382.
(61) Rosenthal, S. J.; Xie, X. L.; Du, M.; Fleming, G. R. *J. Chem. Phys.* **1991**, *95*, 4715.
(62) Maroncelli, M.; Fleming, G. R. *J. Chem. Phys.* **1988**, *88*, 5044.
(63) Castner, E. W., Jr.; Maroncelli, M. *J. Mol. Liq.* **1998**, *77*, 1.
(64) Barbara, P. F.; Walker, G. C.; Smith, T. P. *Science* **1992**, *256*, 975.
(65) Barbara, P. F.; Jarzeba, W. *Adv. Photochem.* **1990**, *15*, 1.
(66) Bhasikuttan, A. C.; Suzuki, M.; Nakashima, S.; Okada, T. *J. Am. Chem. Soc.* **2002**, *124*, 8398.
(67) Damrauer, N. H.; Cerullo, G.; Yeh, A.; Boussie, T. R.; Shank, C. V.; McCusker, J. K. *Science* **1997**, *275*, 54.
(68) Owrutsky, J. C.; Raftery, D.; Hochstrasser, R. M. *Annu. Rev. Phys. Chem.* **1994**, *45*, 519.
(69) Lian, T.; Bromberg, S. E.; Asplund, M.; Yang, H.; Harris, C. B. *J. Phys. Chem.* **1996**, *100*, 11994.
(70) Dougherty, T. P.; Heilweil, E. J. *Chem. Phys. Lett.* **1994**, *227*, 19.
(71) Asbury, J. B.; Wang, Y.; Lian, T. *Bull. Chem. Soc. Jpn.* **2002**, *75*, 973.
(72) Worl, L. A.; Duesing, R.; Chen, P.; Ciana, L. D.; Meyer, T. J. *J. Chem. Soc., Dalton Trans.* **1991**, 849.
(73) Marcus, R. A. On the theory of ion transfer rates across the interface of two immiscible liquids. *J. Chem. Phys.* **2000**, *113*, 1618.
(74) Gao, Y. Q.; Georgievskii, Y.; Marcus, R. A. *J. Chem. Phys.* **2000**, *112*, 3358.
(75) Gao, Y. Q.; Marcus, R. A. *J. Chem. Phys.* **2000**, *113*, 6351.
(76) Gosavi, S.; Marcus, R. A. *J. Phys. Chem. B* **2000**, *104*, 2067.
(77) Pankove, J. I. *Optical Processes in Semiconductors*; Dover: New York, 1975.
(78) Zaban, A.; Ferrere, S.; Sprague, J.; Gregg, B. A. *J. Phys. Chem. B* **1997**, *101*, 55.
(79) Heimer, T. A.; Bignozzi, C. A.; Meyer, G. J. *J. Phys. Chem.* **1993**, *97*, 11987.
(80) Argazzi, R.; Bignozzi, C. A.; Heimer, T. A.; Castellano, F. N.; Meyer, G. J. *Inorg. Chem.* **1994**, *33*, 5741.
(81) Sauve, G.; Cass, M. E.; Coia, G.; Doig, S. J.; Lauermann, I.; Pomykal, K. E.; Lewis, N. S. *J. Phys. Chem. B* **2000**, *104*, 6821.
(82) Vlachopoulos, N.; Liska, P.; Augustynski, J.; Gratzel, M. *J. Am. Chem. Soc.* **1988**, *110*, 1216.
(83) O'Regan, B.; Moser, J.; Anderson, M.; Gratzel, M. *J. Phys. Chem.* **1990**, *94*, 8720.
(84) Casper, J. V.; Westmoreland, T. D.; Allen, G. H.; Bradley, P. G.; Meyer, T. J.; Woodruff, W. H. *J. Am. Chem. Soc.* **1984**, *106*, 3492.
(85) Zaban, A.; Ferrere, S.; Gregg, B. A. *J. Phys. Chem. B* **1998**, *102*, 452.
(86) Lyon, L. A.; Hupp, J. T. *J. Phys. Chem. B* **1999**, *103*, 4623.
(87) Rothenberger, G.; Fitzmaurice, D.; Gratzel, M. *J. Phys. Chem.* **1992**, *96*, 5983.
(88) Redmond, G.; Fitzmaurice, D. *J. Phys. Chem.* **1993**, *97*, 1426.
(89) Enright, B.; Redmond, G.; Fitzmaurice, D. *J. Phys. Chem.* **1994**, *98*, 6195.
(90) Yamakata, A.; Ishibashi, T.-a.; Onishi, H. *Chem. Phys. Lett.* **2001**, *333*, 271.
(91) Seeger, K. *Semiconductor Physics: an introduction*, 5th ed.; Springer: Berlin, Germany, 1990; Vol. 40.
(92) Lu, H.; Prieskorn, J. N.; Hupp, J. T. *J. Am. Chem. Soc.* **1993**, *115*, 4927.
(93) Blackbourn, R. L.; Johnson, C. S.; Hupp, J. T. *J. Am. Chem. Soc.* **1991**, *113*, 1060.
(94) Marcus, R. A.; Sutin, N. *Biochim. Biophys. Acta* **1985**, *811*, 265.
(95) Becka, A. M.; Miller, C. J. *J. Phys. Chem.* **1992**, *96*, 2657.
(96) Enright, B.; Fitzmaurice, D. *J. Phys. Chem.* **1996**, *100*, 1027.
(97) Nazeeruddin, M. K.; Zakeerudin, S. M.; Humphry-Baker, R.; Jirousek, M.; Liska, P.; Vlachopoulos, N.; Shklover, V.; Fischer, C.-H.; Gratzel, M. *Inorg. Chem.* **1999**, *38*, 6298.
(98) Yan, S. G.; Hupp, J. T. *J. Phys. Chem.* **1996**, *100*, 6867.
(99) Marcus, R. A. *J. Phys. Chem.* **1990**, *94*, 1050.
(100) Marcus, R. A. *J. Chem. Phys.* **1965**, *43*, 679.
(101) Liu, Y. P.; Newton, M. D. *J. Phys. Chem.* **1994**, *98*, 7162.
(102) Yonemoto, E. H.; Saupe, G. B.; Schmehl, R. H.; Hubig, S. M.; Riley, R. L.; Iverson, B. L.; Mallouk, T. E. *J. Am. Chem. Soc.* **1994**, *116*, 4786.